Internal Composition versus the Mechanical Properties of Polyelectrolyte Multilayer Films: The Influence of Chemical Cross-Linking

ARTICLE *in* LANGMUIR · DECEMBER 2009

Impact Factor: 4.46 · DOI: 10.1021/la9018663 · Source: PubMed

Langmuir
Article
pubs.acs.org/Langmuir

Internal Composition versus the Mechanical Properties of Polyelectrolyte Multilayer Films: The Influence of Chemical Cross-Linking†

Thomas Boudou,‡ Thomas Crouzier,§ Rachel Auzély-Velty,∥ Karine Glinel,⊥ and Catherine Picart*,‡,§

‡Minatec, Grenoble Institute of Technology and LMGP, 3 parvis Louis Néel, F-38016 Grenoble Cedex, France, §Dynamique des Interactions Membranaires Normales et Pathologiques, Université de Montpellier 2 et 1, CNRS, Place Eugène Bataillon, F-34095 Montpellier Cedex 5, France, ∥Centre de Recherches sur les Macromolécules Végétales (CERMAV-CNRS and Université Joseph Fourier), BP53, F-38 041 Grenoble Cedex 9, France, and ⊥Laboratoire Polymères, Biopolymères, Surfaces, Université de Rouen − CNRS, Bd Maurice de Broglie, F-76821 Mont-Saint-Aignan, France.

Received May 25, 2009. Revised Manuscript Received August 19, 2009

Different types of polyelectrolyte multilayer films composed of poly(L-lysine)/hyaluronan (PLL/HA), chitosan/hyaluronan (CHI/HA) and poly(allylamine hydrochloride)/poly(L-glutamic acid) (PAH/PGA) have been investigated for their internal composition, including water content, ion pairing, and ability to be covalently cross-linked, as well as for their mechanical properties. Film buildup under physiological conditions was monitored by the quartz crystal microbalance with dissipation monitoring (QCM-D) and attenuated total reflectance Fourier transform infrared spectroscopy (ATR-FTIR), which allows unambiguous quantification of the different groups present in the polyelectrolytes. (PAH/PGA) films emerged as the most dense films with the lowest hydration (29%) and the highest COO^- molar density. In addition, PAH is greatly in excess in these films (3 PAH monomers per PGA monomer). The formation of amide bonds during film cross-linking using the water-soluble carbodiimide EDC was also investigated. All of the films could be cross-linked in a tunable manner, but PAH/PGA exhibited the highest absolute number of amide bonds created, ∼7 times more than for (PLL/HA) and (CHI/HA) films. The Young's modulus E of the films measured by AFM nanoindentation was shown to vary over 1 to 2 orders of magnitude for the different systems. Interestingly, a linear relationship between E and the density of the covalent cross-links created was observed for (PLL/HA) and (CHI/HA) films whereas (PGA/PAH) films exhibited biphasic behavior. The mean distance between covalent cross-links was estimated to be ∼11 nm for (PLL/HA) and (CHI/HA) films and only ∼6 nm for (PAH/PGA) films for the maximum EDC concentration tested (100 mg/mL).

Introduction

Polyelectrolyte multilayer films (PEMs) are obtained by alternately depositing polyelectrolytes onto a substrate. They are the subject of an increasing number of studies[1−3] both at a fundamental level, for understanding the mechanisms underlying film buildup, internal structure, and hydration,[1] and also for specific applications in various fields of materials science. These include, among others, antireflection coatings,[4] filtration membranes,[5] superhydrophobic coatings,[6] antibacterial coatings,[7] and biomaterial coatings.[8]

Many fundamental studies use poly(allylamine hydrochloride)/poly(styrene sulfonate) (PAH/PSS) films as a "model" system, probably because this system was the first to be investigated.[9] Its thickness is known to grow linearly with the number of deposited layers.[10] Also—and this is a key advantage—PSS can be deuterated, which allows the internal structure to be probed by neutron reflectometry. Last, the charge matching and internal cohesion of these films are high, so they can resist harsh conditions. Their processing or post-treatment in high salt concentrations is thus possible.[11,12] In such films, the percentage of trapped counterions appears to remain low.[13] However, more and more polyelectrolyte films are found to show superlinear or exponential growth. This was initially observed for polysaccharides and/or polypeptide films[14,15] built under physiological conditions (ionic strength of 0.15 M NaCl, neutral pH) as well as for films made of synthetic polyelectrolytes built at high ionic strength.[16] However, this type of growth mode is now commonly observed for many kinds of synthetic polyelectrolytes[17] and even for composite organic/inorganic films containing clay platelets.[18] So far, in

† Part of the "Langmuir 25th Year: Molecular and macromolecular self-assemblies" special issue.

*Corresponding author. E-mail: catherine.picart@minatec.grenoble-inp.fr. Phone: +33(0)4 56 52 93 11. Fax: +33(0)4 56 52 93 01.

(1) Von Klitzing, R. *Phys. Chem. Chem. Phys.* **2006**, *8*, 5012–5033.
(2) Decher, G. *Science* **1997**, *277*, 1232–1237.
(3) Tang, Z.; Wang, Y.; Podsiadlo, P.; Kotov, N. A. *Adv. Mater.* **2006**, *18*, 3203–3224.
(4) Hiller, J. A.; Mendelsohn, J. D.; Rubner, M. F. *Nat. Mater.* **2002**, *1*, 59–63.
(5) Miller, M. D.; Bruening, M. L. *Chem. Mater.* **2005**, *17*, 5375–5381.
(6) Ji, J.; Fu, J.; Shen, J. *Adv. Mater.* **2006**, *18*, 1441–1444.
(7) Dai, J.; Bruening, M. L. *Nano Lett.* **2002**, *2*, 497–501.
(8) Schultz, P.; Vautier, D.; Richert, L.; Jessel, N.; Haikel, Y.; Schaaf, P.; Voegel, J.-C.; Ogier, J.; Debry, C. *Biomaterials* **2005**, *26*, 2621–2630.
(9) Korneev, D.; Lvov, Y. M.; Decher, G.; Schmitt, J.; Yaradaikin, S. *Physica B* **1995**, *213-214*, 954–956.
(10) Decher, G.; Lvov, Y. M.; Schmitt, J. *Thin Solid Films* **1994**, *244*, 772–777.
(11) Blomberg, E.; Poptoshev, E.; Caruso, F. *Langmuir* **2006**, *22*, 4153–4157.
(12) Lebedeva, O. V.; Kim, B.-S.; Vasilev, K.; Vinogradova, O. I. *J. Colloid Interface Sci.* **2005**, *284*, 455–462.
(13) Jaber, J. A.; Schlenoff, J. B. *Langmuir* **2007**, *23*, 896–901.
(14) Picart, C.; Lavalle, P.; Hubert, P.; Cuisinier, F. J. G.; Decher, G.; Schaaf, P.; Voegel, J.-C. *Langmuir* **2001**, *17*, 7414–7424.
(15) Lavalle, P.; Gergely, C.; Cuisinier, F. J. G.; Decher, G.; Schaaf, P.; Voegel, J.-C.; Picart, C. *Macromolecules* **2002**, *35*, 4458–4465.
(16) Ruths, J.; Essler, F.; Decher, G.; Riegler, H.; Polyelectrolytes, I. *Langmuir* **2000**, *16*, 8871–8878.
(17) Zacharia, N. S.; DeLongchamp, D. M.; Modestino, M.; Hammond, P. T. *Macromolecules* **2007**, *40*, 1598–1603.
(18) Podsiadlo, P.; Michel, M.; Lee, J.; Verploegen, E.; Wong Shi Kam, N.; Ball, V.; Lee, J.; Qi, Y.; Hart, J.; Hammond, P. T.; Kotov, N. A. *Nano Lett.* **2008**, *8*, 1762–1770.

addition to the well-known fact that polyelectrolytes can diffuse[19] and exchange with other polyelectrolytes within PEM,[20] very little is known about the internal composition, including charge pairing, polyelectrolyte stoichiometry, and molar densities, of such films. We applied a quantitative method, attenuated total reflection Fourier transform infrared spectroscopy (ATR-FTIR), to analyze ion pairing in situ in PEM films during film buildup under physiological conditions.[21,22] In particular, we applied it to obtain information about the internal composition of films containing polysaccharides with either carboxylic or sulfate groups. This included hyaluronan, chondrotin sulfate, and heparin paired with poly(L-lysine) (PLL) as the polycation. Our results evidenced significant nonstoichiometry in such films with a $\sim$ 2:1 monomer ratio, the polycation (in this case, PLL) being in excess. Understanding how polyelectrolytes interact in exponentially growing films and the exact composition of the film is thus of paramount importance for gaining insight into these new model films. This will also be useful for the preparation of films with targeted properties. Independently of the exponential growth, an additional feature of PEM that has emerged during the last 10 years is the possibility of modifying their mechanical properties. This will have an impact on several other film properties such as stress resistance, (bio)degradation, and aging. The mechanical properties can be modified by changing the ratio of ionic cross-links through pH or ionic strength adjustment.[23] In addition, several methods have been proposed for introducing covalent cross-links into the films. These include heating at high temperature,[24] using carbodiimide chemistry to create covalent amide bonds,[25−27] introducing thiol-grafted polyelectrolytes to form disulfide bridges[28] or photoreactive polyelectrolytes,[29,30] and, more recently, click chemistry.[31] To measure the mechanical properties of the films in their liquid state quantitatively, there are few methods that can be applied to thin films. This category includes AFM nanoindentations,[32] piezorheometry,[33] capillary wave,[34] and bulging tests.[35] So far, the relationship between a film's internal composition and mechanical properties has never been systematically investigated, although PEM stiffness is now recognized as an important parameter that has an influence on cellular processes such as adhesion and differentiation.[36−38]

The aim of the present work was to obtain further insight into the internal composition of PEM films undergoing exponential growth. These films are built in a salt-containing solution with no intermediate water rinse or drying, a process that can influence film formation. For this purpose, three different types of films made of synthetic polyelectrolytes, polysaccharides, or polypeptides were selected, and their cross-linking using carbodiimide chemistry was investigated. Poly(L-lysine)/hyaluronan (PLL/HA),[14] chitosan/hyaluronan (CHI/HA),[39] and poly(allylamine hydrochloride)/poly(L-glutamic acid) (PAH/PGA) films[40] (Figure 1) were chosen because they are known to grow exponentially under physiological conditions. In addition, for (PLL/HA) films, we recently demonstrated that the degree of cross-linking can be varied in a tunable manner by controlling the concentration of cross-linker brought into contact with the films after their preparation.[37]

Quartz crystal microbalance with dissipation monitoring (QCM-D) was employed to obtain information on the hydrated thickness and to deduce the degree of hydration of the deposited layers. ATR-FTIR spectroscopy was used to obtain information on the film's internal chemical structure as well as on ion pairing.[22,41] It allowed specific chemical groups to be monitored. We identified and quantified each polyelectrolyte by the chemical signature of one of its groups. One exception was PAH, which was not very visible with FTIR spectroscopy and which was thus quantified by microfluorimetry. Furthermore, we used an established cross-linking protocol based on carbodiimide chemistry[27] that selectively couples carboxylic and amine groups to create amide bonds. We quantified the molar density of the covalent cross-links in the films. In a gel, the density of cross-links is known to determine the gel's mechanical properties. Here, we attempted to find a relationship between the density of chemical cross-links in the films and their mechanical properties. For this, we employed nanoindentation experiments using colloidal probe AFM[32] to measure the Young's moduli of the film at different degrees of cross-linking.

Materials and Methods

Chemicals. Polyelectrolytes of commercial origin were used for the buildup of the polyelectrolyte architectures. PAH (cat no. 28,322-3, 5×10^4 g/mol, molecular weight (MW) of the monomeric unit 58 g/mol) was purchased from Aldrich. Fluorescein isothiocyanate (FITC)-labeled PAH was synthesized, as described previously,[42] by mixing FITC and PAH in 0.05 M borate buffer, followed by dialysis against pure water. PGA (P4886, 4.5×10^4 g/mol, molar mass of the monomer unit 128 g/mol) and PLL (P2636, 7×10^4 g/mol, MW of the monomer unit 129 g/mol) were purchased from Sigma. HA (3.6×10^5 g/mol, molar mass of the monomer unit 378 g/mol) was purchased from Lifecore Biomedical, and CHI (5×10^3 g/mol, molar mass of the monomer unit 165 g/mol) was purchased from Medipol (according to the manufacturer, the supplied degree of acetylation (DA) is less than 10%). For the (PAH/PGA) and (PLL/HA) films,

(19) Picart, C.; Mutterer, J.; Richert, L.; Luo, Y.; Prestwich, G. D.; Schaaf, P.; Voegel, J.-C.; Lavalle, P. *Proc. Natl. Acad. Sci. U.S.A.* **2002**, *99*, 12531–5.
(20) Boulmedais, F.; Bozonnet, M.; Schwinte, P.; Voegel, J.-C.; Schaaf, P. *Langmuir* **2003**, *19*, 9873–9882.
(21) Crouzier, T.; Picart, C. *Biomacromolecules* **2009**, *10*, 433–42.
(22) Sukhishvili, S. A.; Granick, S. *Macromolecules* **2002**, *35*, 301–310.
(23) Jaber, J. A.; Schlenoff, J. B. *J. Am. Chem. Soc.* **2006**, *128*, 2940–7.
(24) Harris, J. J.; DeRose, P. M.; Bruening, M. L. *J. Am. Chem. Soc.* **1999**, *121*, 1978–1979.
(25) Schuetz, P.; Caruso, F. *Adv. Funct. Mater.* **2003**, *13*, 929–937.
(26) Yang, S. Y.; Lee, D.; Cohen, R. E.; Rubner, M. F. *Langmuir* **2004**, *20*, 5978–5981.
(27) Richert, L.; Boulmedais, F.; Lavalle, P.; Mutterer, J.; Ferreux, E.; Decher, G.; Schaaf, P.; Voegel, J.-C.; Picart, C. *Biomacromolecules* **2004**, *5*, 284–94.
(28) Li, B.; Rozas, J.; Haynie, D. T. *Biotechnol. Prog.* **2006**, *22*, 111–117.
(29) Pozos Vazquez, C.; Boudou, T.; Dulong, V.; Nicolas, C.; Picart, C.; Glinel, K. *Langmuir* **2009**, *25*, 3556–3563.
(30) Olugebefola, S. C.; Ryu, S.-W.; Nolte, A. J.; Rubner, M. F.; Mayes, A. M. *Langmuir* **2006**, *22*, 5958–62.
(31) Such, G. K.; Quinn, J. F.; Quinn, A.; Tjipto, E.; Caruso, F. *J. Am. Chem. Soc.* **2006**, *128*, 9318–9319.
(32) Richert, L.; Engler, A. J.; Discher, D. E.; Picart, C. *Biomacromolecules* **2004**, *5*, 1908–16.
(33) Collin, D.; Lavalle, P.; Garza, J. M.; Voegel, J.-C.; Schaaf, P.; Martinoty, P. *Macromolecules* **2004**, *37*, 10195–10198.
(34) Safouane, M.; Miller, R.; Möhwald, H. *J. Colloid Interface Sci.* **2005**, *292*, 86–92.
(35) Lin, Y.-H.; Jiang, C.; Xu, J.; Lin, Z.; Tsukruk, V. V. *Adv. Mater.* **2007**, *19*, 3827–3832.
(36) Ren, K.; Crouzier, T.; Roy, C.; Picart, C. *Adv. Funct. Mater.* **2008**, *18*, 1378–1389.
(37) Schneider, A.; Francius, G.; Obeid, R.; Schwinte, P.; Hemmerle, J.; Frisch, B.; Schaaf, P.; Voegel, J.-C.; Senger, B.; Picart, C. *Langmuir* **2006**, *22*, 1193–1200.
(38) Thompson, M. T.; Berg, M. C.; Tobias, I. S.; Rubner, M. F.; Van Vliet, K. J. *Biomaterials* **2005**, *26*, 6836–45.
(39) Richert, L.; Lavalle, P.; Payan, E.; Shu, X. Z.; Prestwich, G. D.; Stoltz, J.-F.; Schaaf, P.; Voegel, J.-C.; Picart, C. *Langmuir* **2004**, *20*, 448–58.
(40) Boulmedais, F.; Ball, V.; Schwinte, P.; Frisch, B.; Schaaf, P.; Voegel, J.-C. *Langmuir* **2003**, *19*, 440–445.
(41) Muller, M.; Brissová, M.; Rieser, T.; Powers, A. C.; Lunkwitz, K. *Mater. Sci. Eng., C* **1999**, *8*−*9*, 163–169.
(42) Volodkin, D. V.; Larionova, N. I.; Sukhorukov, G. B. *Biomacromolecules* **2004**, *5*, 1962–1972.

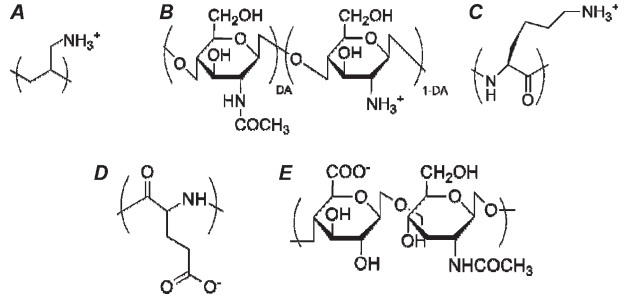

Figure 1. Chemical structures of the polyelectrolytes used in this study. The three polycations with NH_3^+ groups are (A) PAH, (B) CHI, and (C) PLL. The polyanions with COO^- groups are (D) PGA and (E) HA.

the polyelectrolyte solutions were dissolved at 1 mg/mL in Hepes−NaCl buffer (20 mM Hepes, 0.15 M NaCl, pH 7.4) except for PLL, which was prepared at 0.5 mg/mL in the same buffer. For the (CHI/HA) films, the polyelectrolyte solutions were used at 1 mg/mL in a sodium acetate−NaCl buffer (0.01 M, 0.15 M NaCl, pH 4.6). During film build up, all of the rinsing steps were performed in the salt-containing solution, and the films were never dried. For microscopic observations and AFM nanoindentations, the films were prepared as previously described[39] using a dipping robot (DR3, Kierstein GmbH, Germany) on 14-mm-diameter glass slides (VWR Scientific, France) previously cleaned with 10 mM SDS and 0.1 M HCl and extensively rinsed.

For the chemical cross-linking of the films, we followed a previously published protocol[27] based on the reaction of activated carboxylic sites with primary amine groups in the presence of 1-ethyl-3-(3-dimethylaminopropyl) carbodiimide (EDC) and of *N*-hydroxysulfo-succinimide (sNHS) (both purchased from Sigma-Aldrich). EDC and sNHS were dissolved in a solution of 0.15 M NaCl at pH 5, and cross-linking was allowed to proceed overnight at 4 °C. The final EDC concentration varied between 2 and 100 mg/mL, and sNHS remained constant at 11 mg/mL. Rinsing was performed three times with the Hepes-NaCl buffer solution for 1 h. All of the solutions were prepared in ultrapure water (Milli Q-plus system, Millipore) except for the FTIR experiments, which required deuterium oxide (Aldrich, cat no. 15,188-2).

Quartz Crystal Microbalance with Dissipation Monitoring (QCM-D). The film buildup was monitored in situ by QCM-D (Q-Sense, Götenborg, Sweden) as already described.[14,21] Briefly, a gold-coated quartz crystal was excited at its fundamental frequency (about 5 MHz, $\nu = 1$) as well as at the third, fifth, and seventh overtones ($\nu = 3$, 5, and 7 corresponding to 15, 25, and 35 MHz, respectively). Changes in the resonance frequencies Δf and in the relaxation of the vibration once the excitation had stopped were measured at the four frequencies. The QCM-D data were analyzed using the Voigt model[43] included in the Qtools software (Q-Sense, Götenborg, Sweden) by assuming and fixing the values of the film density, buffer density, and viscosity. Three parameters (film thickness, viscosity, and shear modulus) were then deduced.

Fourier Transform Infrared Spectroscopy in Attenuated Total Reflection. Film buildup on a ZnSe crystal and its subsequent cross-linking were investigated by in situ FTIR spectroscopy in attenuated total reflection (ATR) mode with a Vertex 70 spectrophotometer (Bruker Optic Gmbh, Ettlingen, Germany). All of the experimental details have been described previously.[21,27,44] The experiments were performed in a deuterated 0.15 M NaCl solution adjusted to pH 7.4 (or 4.6 for (CHI/HA) films). The spectrum from the bare ZnSe crystal in contact with the 0.15 M NaCl solution was taken as the reference. After each polyelectrolyte deposition and rinsing step, a single-channel spectrum from 64 interferograms was recorded between 400 and 4000 cm^{-1} with 2 cm^{-1} resolution using Blackman-Harris three-term apodization and standard Bruker OPUS/IR software v6.5. A final spectrum was also acquired after film cross-linking.

Peak Assignment and Quantification by ATR-FTIR Spectroscopy. For a quantitative analysis of the structure of the films, calibration spectra of the polyelectrolyte solutions in contact with the nonadsorbing crystal were first recorded following previously published protocols.[21,22,45] For PLL, the amide band with two peaks at 1635 and 1670 cm^{-1}, attributed to random and turn structures, respectively,[20,21] was visible (Figure SI 1A).

For PGA, we observed two carboxylic peaks at 1563 and 1405 cm^{-1} as well as an amide I band. As previously described by Boulmedais et al.,[40] three components centered at 1630, 1645, and 1665 cm^{-1} were observed. These peaks corresponded to α-helix, random coil, and turn structures, respectively (Figure 2A). In the CHI spectrum, the most intense peaks characteristic of the saccharide rings[46] were observed at 1080 and 1040 cm^{-1} (Figure 2B). Because the HA spectrum also exhibited these saccharide peaks (Figure 2C), the increase in the peak for each CHI layer was calculated by subtracting its value for the CHI_i layer from its value for the HA_{i-1} layer. The total CHI content was thus calculated after finding the sum contribution of each layer.

For HA, the carboxylic peaks at 1610 and 1414 cm^{-1}, the amide band in the 1635 cm^{-1} region, and the peaks of saccharide rings in the 950−1100 cm^{-1} region were observed as previously described (Figure 2C).[21,37] The signal ranging from 1700 to 1525 cm^{-1} composed of both carboxylic (around 1610 cm^{-1}) and amide I (at 1640 cm^{-1}) bands was deconvoluted for the quantitative analysis. Residual water removal, baseline correction, and deconvolution were achieved with Opus software. The most consistent results were obtained when the amide band was assumed to be Gaussian, the COO^- band was assumed to be 70% Lorenzian and 30% Gaussian, and the saccharide band was assumed to be 40% Lorenzian and 60% Gaussian.

Finally, in the case of PAH, no peak could be clearly identified. We thus quantified PAH^{FITC} adsorption using a fluorescence microplate reader as described below.

For ATR-FTIR quantification of the adsorbed amounts of polyelectrolyte, the penetration depth of the evanescent wave, d_P, and the calibration constant K given below were required

$$d_P = \frac{\lambda}{2\pi n_1 \left[\sin^2(\theta) - \left(\frac{n_2}{n_1}\right)^2\right]^{1/2}} \quad (1)$$

In eq 1, λ is the wavelength of the incident light, θ is the incident angle (45°), and n_1 and n_2 are the refractive indexes of the ZnSe crystal and medium, respectively ($n_1 = 2.42$ and $n_2 = 1.34$). In the case of an infinite medium, absorbance A can be derived:

$$A = KC \text{ with } K = \frac{n_2}{n_1}\frac{\varepsilon}{\cos\theta}\frac{d_P}{2} \quad (2)$$

The calibration constant K was determined for specific peaks: a saccharide peak for CHI, the COO^- peak for PGA and HA, and the amide band for PLL (Table 1). For this, polyelectrolyte solutions of known concentrations were brought into contact with a nonadsorbing bare ZnSe crystal as previously described.[21,22,47] From the slope of the absorbance for a given band, the constant K was obtained for each polyelectrolyte (data not shown and Table 1). However, for technical reasons it was not possible to get

(43) Voinova, M. V.; Rodahl, R.; Jonson, R.; Kasemo, B. *Phys. Scr.* **1999**, *59*, 391–396.
(44) Schwinté, P.; Voegel, J.-C.; Picart, C.; Haikel, Y.; Schaaf, P.; Szalontai, B. *J. Phys. Chem. B* **2001**, *105*, 11906–11916.
(45) Frantz, P.; Granick, S. *Macromolecules* **1995**, *28*, 6915–6925.
(46) Picart, C.; Schneider, A.; Etienne, O.; Mutterer, J.; Schaaf, P.; Egles, C.; Jessel, N.; Voegel, J.-C. *Adv. Funct. Mater.* **2005**, *15*, 1771–1780.
(47) Xie, A. F.; Granick, S. *Macromolecules* **2002**, *35*, 1805–1813.

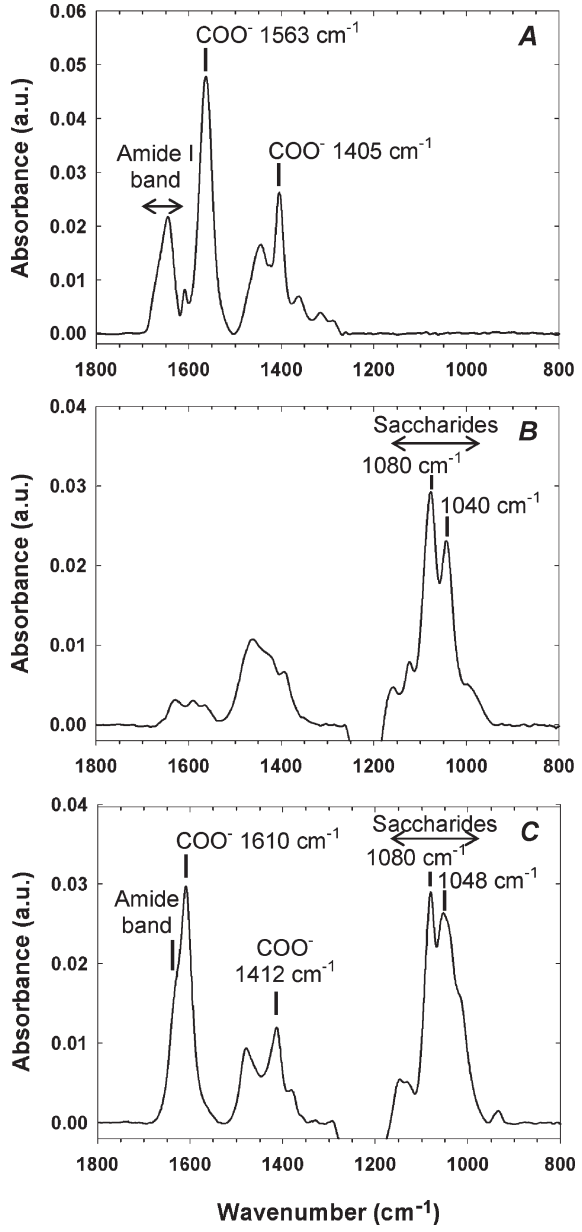

Figure 2. FTIR calibration spectra measured from polyelectrolyte solutions and major peak assignments. FTIR spectra of PGA at 12.5 mg/mL (pH 7.4) (A), CHI at 15 mg/mL (pH 4.6) (B), and HA at 15 mg/mL (C) (pH 4.6) are shown with the peaks used for quantification.

absorbance values as high as those obtained during the film buildup (0.1 versus 1 maximum, respectively). Thus, we assumed that the calibration curve could be extrapolated to higher absorbance values, similarly to previously established procedures.[22,45] To quantify the buildup of the PEM, analyses were always performed after rinsing each layer in order to obtain only the contribution of the adsorbed polyelectrolytes.

The expression of the absorbance of an adsorbed dry film of finite thickness, t_{DF}, can be derived from the optical equations given by Harrick[48]

$$A = K\frac{n_2'}{n_2}\rho_F\left(1-\exp\left(-2\frac{t_{DF}}{d_P}\right)\right) = K\frac{n_2'}{n_2}\rho_F F(t_{DF}/d_P) \quad (3)$$

(48) Harrick, N. J. *Internal Reflection Spectroscopy*; Interscience Publishers: New York, 1967.

Table 1. Nature of the Chemical Bonds Recorded by ATR-FTIR for Each Polyelectrolyte with the Corresponding Wavenumber, Penetration Depth d_p, and Calibration Factor K

chemical bond	wavenumber (cm^{-1})	d_p (nm)	K (Abs/(mg/mL))
PLL C=O (amide I)	1635	914.7	4.66×10^{-3}
PLL C=O (amide I)	1670	895.5	0.71×10^{-3}
HA COO^-	1610	929.9	1.80×10^{-3}
CHI saccharide (pH 4.6)	1080	1384.7	1.85×10^{-3}
HA COO^- (pH 4.6)	1610	929.9	1.91×10^{-3}
PGA COO^-	1563	956.8	4.30×10^{-3}

where n_2' is the refractive index of the film (taken to be 1.38 for each film[49]) and ρ_F is the film density. In our experiments, the penetration depth of the evanescent wave was large ($\sim$1 μm) in relation to the "dry" thickness of the multilayers (around 100 nm at most), and $F(t_{DF}/d_p)$ increased only weakly with t_{DF}/d_p. Thus, a linear approximation for the $F(t_{DF}/d_p)$ function was used with a slope of 1.81.[21] Accordingly, the adsorbed amount $\Gamma = \rho_F t_{DF}$ (expressed in $\mu g/cm^2$) is simply given by

$$\Gamma = \frac{n_2}{n_2'}\frac{d_P}{1.81K}A \quad (4)$$

Molar Density and Monomer Ratio. The molar density (based on the monomeric unit) was derived by dividing the adsorbed amounts (determined from the ATR-FTIR individual spectra) by the molar mass of the monomer and the hydrated film thickness measured by QCM-D.

The ratio of polyanion over polycation monomers at each deposit step was calculated for each film type by dividing the absolute number of polyanion monomers by that of the polycation monomers. This was achieved by ATR-FTIR decomposing the selected bands (Table 1) when the calibration factor K and the molecular mass of the monomers were known.

Quantification by Microfluorimetry. The amount of adsorbed PAH was quantified using a fluorescence microplate reader. PEM films were built in situ in 96-well plates by the alternate deposition of PAH^{FITC} and PGA, and the fluorescence intensity of the film was measured after each PAH deposition step using an Infinite M1000 apparatus (TECAN, Austria) with excitation at 494 $\pm$ 10 nm and emission at 518 $\pm$ 10 nm. For quantification, the fluorescence intensity of known amounts of PAH^{FITC} in solution was measured, and a calibration curve was established (calibration factor $K = 7.74 \times 10^3\ I_F/\mu g$, with I_F being the fluorescence intensity in arbitrary units).

Atomic Force Microscopy (AFM). All AFM measurements were carried out in Hepes−NaCl buffer (except for (CHI/HA) in acetate−NaCl buffer) using a Nanoscope V AFM (Veeco). The spring constant of each cantilever was determined using the thermal noise method.[50] Force−indentation profiles were recorded using borosilicate sphere-tipped cantilevers with a radius of $R = 2.5\ \mu m$ (Bioforce Nanoscience) and a spring constant of 60 mN/m. The Young's moduli E were extracted from the above profiles using the finite-thickness-corrected Hertz sphere model.[51] All PEM films were assumed to be incompressible (Poisson's ratio fixed at 0.5). The expression for the indentation force is thus

$$F = \frac{16E}{9}R^{1/2}\delta^{3/2}[1 + 1.133\chi + 1.283\chi^2 + 0.769\chi^3 + 0.0975\chi^4] \quad (5)$$

(49) Richert, L.; Arntz, Y.; Schaaf, P.; Voegel, J.-C.; Picart, C. *Surf. Sci.* **2004**, *570*, 13–29.

(50) Butt, H.-J.; Jaschke, M. *Nanotechnology* **1995**, *6*, 1–7.

(51) Dimitriadis, E. K.; Horkay, F.; Maresca, J.; Kachar, B.; Chadwick, R. S. *Biophys. J.* **2002**, *82*, 2798–810.

where $\chi = (R\delta)^{1/2}/t_{WF}$, t_{WF} is the film's hydrated thickness, and δ is the indentation. δ is obtained by subtracting the deflection d from the movement of the piezoelectric ceramic ($\Delta z = z - z_0$) in the z direction, where z_0 is the contact point determined by following the method proposed by Crick and Yin.[52] To avoid large strain effects, the force−indentation curves were analyzed for micrometer-thick films in the 0−50 nm indentation domain. For each sample probed, two measurements were taken at five positions on two different PEM-coated slides. A perfect overlap of two successive indentations performed at each position was obtained, which indicates that the samples were only elastically and not plastically deformed. Young's moduli were calculated by least-squares fitting of the experimental force−indentation curves.

Results and Discussion

Film Buildup and Hydration. In preliminary experiments, we tested different polyelectrolyte films for their growth properties and compared their cross-linking. We looked for conditions where films could be sufficiently thick after a limited number of depositing steps (typically 8 layer pairs) and for which the extent of cross-linking could be tuned over a wide range of EDC concentration. Under these conditions, exponentially growing (PLL/PGA)[15] and (PLL/alginate)[53] films were eliminated because their degree of cross-linking was already very high even for low EDC concentrations (data not shown). We thus selected three different types of films that grow exponentially, namely, (PAH/PGA), (CHI/HA) and (PLL/HA) films. Figure 3 shows the evolution of the fundamental frequency shift Δf_1 and the corresponding thickness during the buildup of the three types of films for up to eight layer pairs. For (PAH/PGA) and (CHI/HA) films, similar behavior characterized by good overlap of the normalized $\Delta f/\nu$ curves over the whole range was noted (Figure SI 2). This strongly indicates that these PEMs are predominantly elastic rather than viscous. Conversely, the normalized frequency shifts did not overlap for (PLL/HA) films as previously observed,[14] which is characteristic of viscoelastic behavior that can be described by the Voinova model.[43] Film thickness and the adsorbed amounts deduced from the Voinova model are given in Figure 3 and Table 2, respectively. Of note, similar results were obtained for (PAH/PGA) and (CHI/HA) films by applying the Sauerbrey equation[54] (data not shown), which constitutes a reasonable approximation of the case of rigid films. In the Hepes−NaCl buffer, the $(PLL/HA)_8$ film thickness reached 509 ± 90 nm followed by $(PAH/PGA)_8$ films at 424 ± 43 nm, whereas the thickness of the $(CHI/HA)_8$ film in the acetate−NaCl buffer was slightly lower at 347 ± 45 nm (Figure 3B). Of note, all of the film thicknesses could be fitted by an exponential function. The corresponding adsorbed amounts were higher for $(PLL/HA)_8$ films at 53.4 ± 9.5 $\mu g/cm^2$ than for $(PAH/PGA)_8$ (37.4 ± 7.8 $\mu g/cm^2$) and for $(CHI/HA)_8$ films (37.7 ± 4.9 $\mu g/cm^2$) (Table 2).

It is now acknowledged that solvent molecules contribute to the QCM-D signal[55] whereas infrared spectroscopy is sensitive only to the chemical signature of the polyelectrolyte backbone. Consequently, it senses only the dry film mass.[56] Thus, ATR-FTIR spectra of the same films were acquired in situ for films built on the ATR crystal (Figure 4). For all of the films, regular growth was observed and the different peaks identified during the calibration procedure clearly emerged. For the (PAH/PGA) films (Figure 4A), the amide I band in the 1640 cm^{-1} region and the COO^- peaks at 1563 and 1405 cm^{-1} were particularly visible. At first glance, the absorbance of these films was much higher than for the others.

For (CHI/HA) films (Figure 4B), significant increases in the saccharide peaks, the COO^- peak at 1610 cm^{-1}, and the amide I band were noted. The saccharide peaks increased after each CHI and HA layer was deposited because both polyelectrolytes contributed to the signal, whereas the COO^- peak increased only after each HA deposition step. Importantly, the protonated COOH group at ~1725 cm^{-1} was always negligible and less than 3% of the COO^- peak, indicating that all carboxylic groups were fully ionized. For (PLL/HA) films (Figure 4C), the

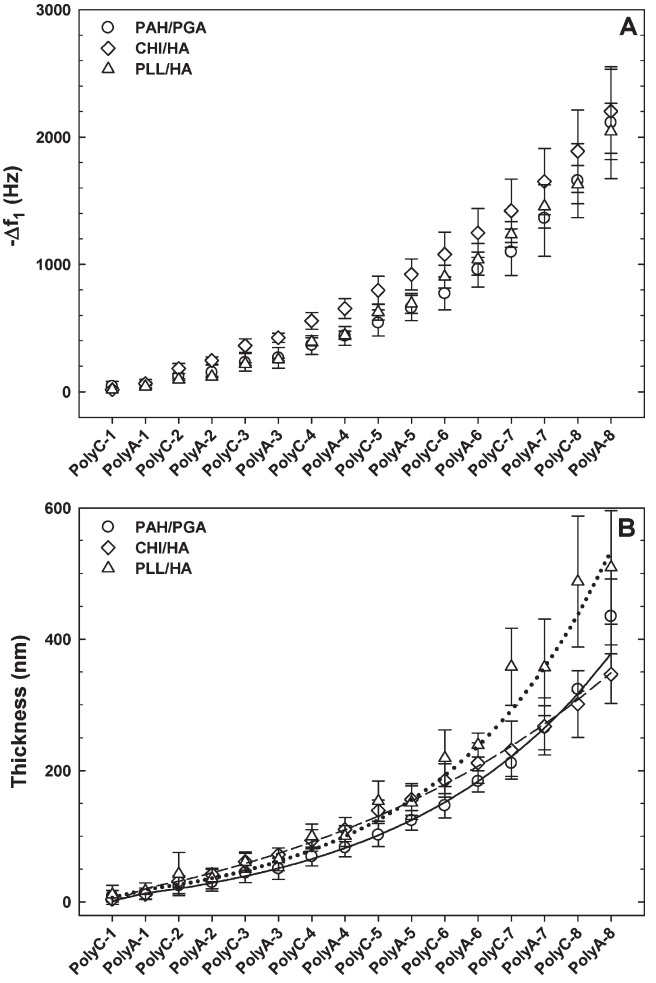

Figure 3. Film growth monitored in situ by QCM-D for (PAH/PGA) (○), (CHI/HA) (◇), and (PLL/HA) (△) films. (A) Difference in the frequency shifts Δf_1 measured at 5 MHz after each polycation and polyanion deposition. (B) Film thickness as a function of the number of deposited layer pairs deduced from the QCM-D data for the three films. PolyC and PolyA refer to polycation and polyanion deposits, respectively. Data were averaged from three different experiments. The experimental data were fitted according to the equation $t_{WF} = a_0 + a_1 \exp(a_2 i_{bil})$, with t_{WF} being the film's hydrated thickness and i_{bil} being the number of layer pairs. The best fits were obtained for $a_0 = -25.9$ nm, $a_1 = 33.5$ nm, and $a_2 = 0.3$ for (PAH/PGA) films (−), $a_0 = -101.7$ nm, $a_1 = 96.5$ nm, and $a_2 = 0.2$ for (CHI/HA) films (---), and $a_0 = -54.0$ nm, $a_1 = 47.7$ nm, and $a_2 = 0.3$ for (PLL/HA) films (···). Data are means ± SD of three independent experiments.

(52) Crick, S. L.; Yin, F. C. *Biomech. Model. Mechanobiol.* **2007**, *6*, 199–210.
(53) Elbert, D. L.; Herbert, C. B.; Hubbell, J. A. *Langmuir* **1999**, *15*, 5355–5362.
(54) Sauerbrey, G. *Z. Phys. A: Hadrons Nucl.* **1959**, *155*, 206–222.
(55) Vörös, J. *Biophys. J.* **2004**, *87*, 553–561.
(56) Krzeminski, A.; Marudova, M.; Moffat, J.; Noel, T. R.; Parker, R.; Wellner, N.; Ring, S. G. *Biomacromolecules* **2006**, *7*, 498–506.

Table 2. Adsorbed Amounts of Polyelectrolyte Determined from ATR-FTIR Spectroscopy (or Microfluorimetry (μfluo) for PAH) and QCM-D Data[a]

	technique	polycation μg/cm^2	polyanion μg/cm^2	total mass μg/cm^2	hydration (% w/w)
$(PAH/PGA)_8$	μfluo-FTIR	13.8	12.7	26.5 ± 1.2	29
	QCM-D	16.5	20.9	37.4 ± 7.8	
$(CHI/HA)_8$	FTIR	3.1	4.0	7.0 ± 1.0	81
	QCM-D	19.1	18.6	37.7 ± 4.9	
$(PLL/HA)_8$	FTIR	3.3	4.3	7.6 ± 0.8	86
	QCM-D	47.6	5.8	53.4 ± 9.5	

[a] Film hydration was calculated from the ratio of total adsorbed amounts.

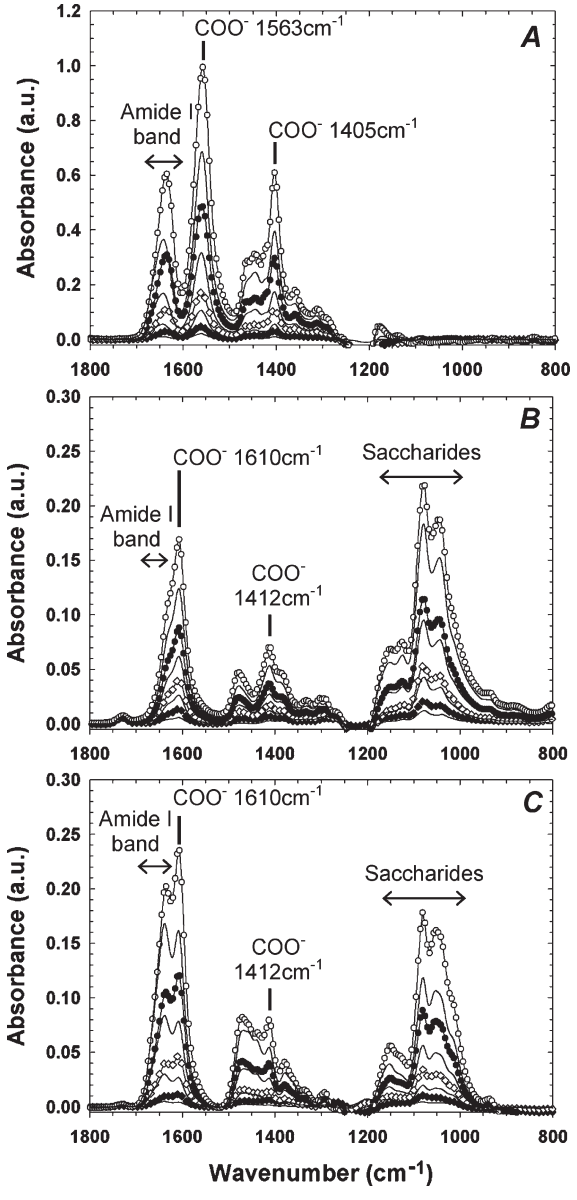

Figure 4. ATR-FTIR spectra acquired during the buildup of (A) $(PAH/PGA)_8$, (B) $(CHI/HA)_8$, and (C) for $(PLL/HA)_8$ films. For clarity, only the absorbance spectra of the polyanion-ended films obtained after the deposition of an even number of layers are shown: 2 (♦), 4 (◊), 6 (●), and 8 (○). The spectra of the polycation-ended films obtained after the deposition of an odd number of layers are represented within continuous lines.

deposition of PLL increased the amide I band in the 1635 cm^{-1} region. Depositions of HA led to an increase in the COO^- peaks (1610 and 1412 cm^{-1}), in the amide I band, and in the saccharide peaks.

From each individual spectrum and from the known calibration constants (Table 1), the amounts of each polyelectrolyte adsorbed were determined. For PAH, the adsorbed amount was determined by microfluorimetry because of the impossibility of quantifying it with ATR-FTIR spectroscopy. These adsorbed amounts are plotted as a function of the number of deposited layers in Figure 5. Similarly to the QCM-D data, the adsorbed amounts obtained from FTIR, although smaller than their QCM counterparts, exhibited exponential growth.

It should be noted that the thickness of the PEM was never enough to entirely contain the evanescent wave because the absorbance values never reached a plateau or showed any sign of curvature change (as a function of the layer number). Our conditions were thus very different from those of Schlenoff et al.,[57] who observed a plateau value in conditions where the penetration depth was about 2 times less than in our case.

Under our conditions, the (PAH/PGA) total adsorbed amounts determined by ATR-FTIR spectroscopy were about 3 times higher than their (PLL/HA) and (CHI/HA) counterparts. Comparison between ATR-FTIR and QCM-D data allowed the film's hydration to be monitored during the buildup (Table 2, Figure 6A). Interestingly, whereas the QCM-D hydrated thicknesses were similar for all of the films, calculating the water content revealed significant differences between the films. In particular, $(PAH/PGA)_8$ films were clearly different with a constant decrease in hydration toward a value of ~29% as compared to ~81% and ~86%, respectively, for $(CHI/HA)_8$ and $(PLL/HA)_8$ films. This latter value is consistent with that found in our recent study.[21] The low hydration of PGA-containing films as compared to HA ones may be due to the different properties of these polyelectrolytes. HA is known to be highly hydrated[58] and in a random coil whereas PGA can be structured in a more compact α-helix. Boulmedais et al. effectively showed for PAH/PGA films that 30% of PGA is structured in an α-helix.[40] Moreover, the charge density of PGA is higher than that of HA (Figure 1).

The molar densities are shown in Figure 5 and given in Table 3 for the films made of eight-layer pairs. For the (CHI/HA) and (PLL/HA) films, they tended to stabilize after three- to four-layer pairs had been deposited. For (PAH/PGA) films, the densities steadily increased as the number of deposited layers increased. Moreover, (PAH/PGA) films exhibited the highest molar density, ~10 times higher than for (PLL/HA) and (CHI/HA) films (respectively 108.5 μmol/cm^3 versus 8.9 μmol/cm^3 and 9.8 μmol/cm^3 for eight-layer pairs).

This qualitatively indicates that (PAH/PGA) films become much more dense than the polysaccharide-containing films. Also, it should be noticed that for all three systems the molar density of the polycation (whether PAH, CHI, or PLL) was always much

(57) Schlenoff, J. B.; Rmaile, A. H.; Bucur, C. B. *J. Am. Chem. Soc.* **2008**, *130*, 13589–13597.
(58) Haxaire, K.; Maréchal, Y.; Milas, M.; Rinaudo, M. *Biopolymers* **2003**, *72*, 149–161.

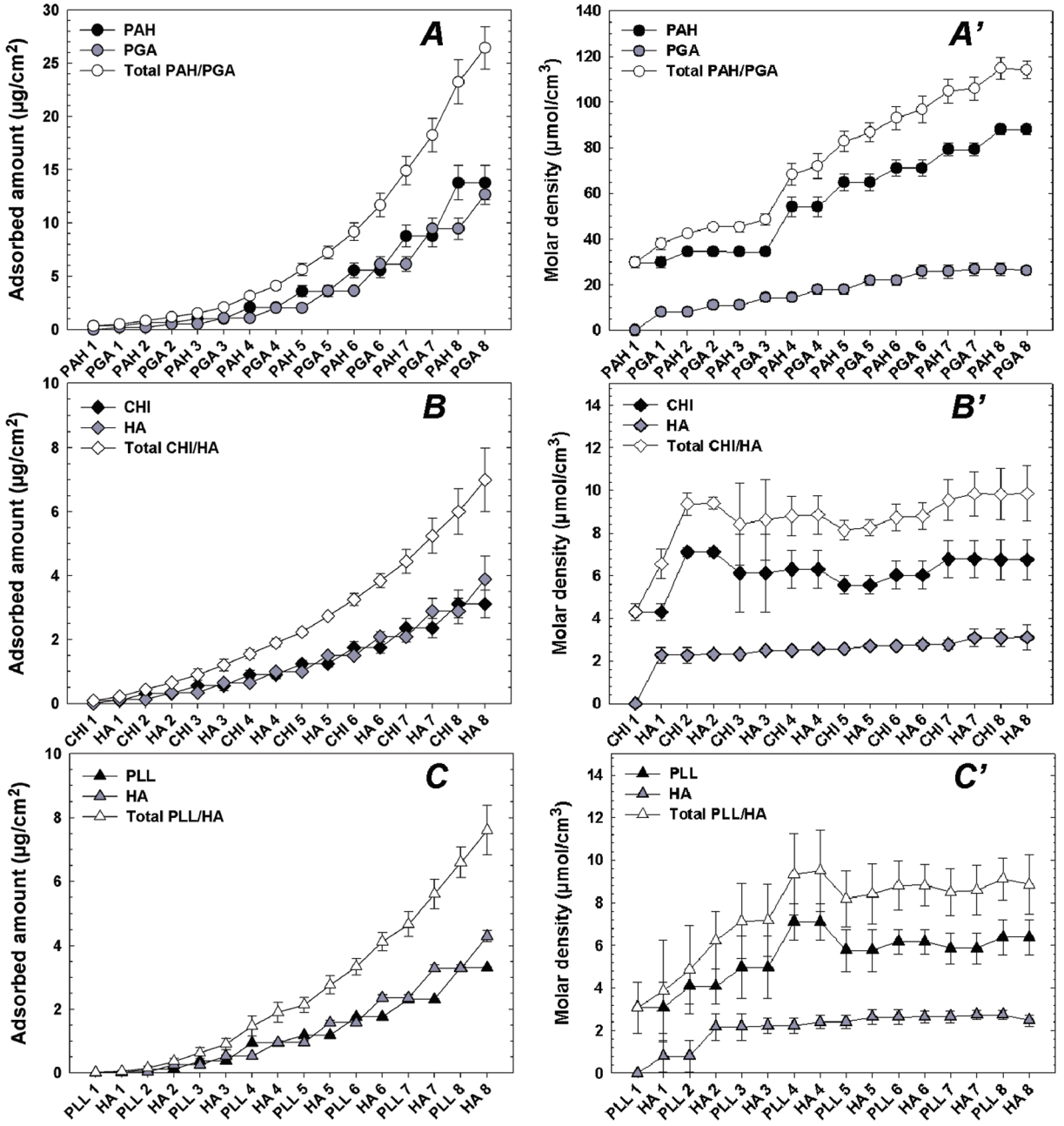

Figure 5. (Left) Adsorbed amounts of polyelectrolyte determined from the ATR-FTIR individual spectra acquired after each layer deposition. (Right) Molar density (based on the monomeric unit) as a function of the number of deposited layers for (A, A′) (PAH/PGA), (B, B′) (CHI/HA), and (C, C′) (PLL/HA). This was calculated by dividing the total adsorbed amounts by the molar mass of the monomer and the film's hydrated thickness as determined by QCM-D. Data are means ± SD of three independent experiments.

greater than that of the polyanion (black versus gray symbols on the curves).

The ratio of polyanion to polycation monomers was also calculated. It is shown in Figure 6 for the different films. This ratio oscillated around a mean value with more pronounced oscillations observed for the (CHI/HA) films. It tended to stabilize toward a mean value of ~0.41 for (PLL/HA) and 0.48 for (CHI/HA) films, indicating that (CHI/HA) contains about 2 polycation monomers per HA unit and (PLL/HA) contains slightly more. This may be related to the diffusive properties of PLL and CHI within (PLL/HA)[21,59,60] and (CHI/HA)[39,61] films, respectively, but also to the structure of the HA monomeric unit. For (PAH/PGA) films, the ratio tended to stabilize around 0.32 ± 0.03, which corresponds to a considerable excess of ~3 PAH monomers per PGA unit. Previous studies by QCM-D on (PAH/PGA) films suggested that PGA chains are predominantly the diffusive species in such films.[40] This was indeed confirmed later by Hübsch et al., who showed that PGA chains can be exchanged for ferrocyanide ions.[62] The fact that PAH has many excess monomers also suggests that it diffuses into the films. This

(59) Picart, C.; Mutterer, J.; Arntz, Y.; Voegel, J.-C.; Schaaf, P.; Senger, B. *Microsc. Res. Tech.* **2005**, *66*, 43–57.
(60) Jourdainne, L.; Lecuyer, S.; Arntz, Y.; Picart, C.; Schaaf, P.; Senger, B.; Voegel, J.-C.; Lavalle, P.; Charitat, T. *Langmuir* **2008**, *24*, 7842–7847.
(61) Schneider, A.; Richert, L.; Francius, G.; Voegel, J.-C.; Picart, C. *Biomed. Mater.* **2007**, *2*, S45–51.
(62) Hübsch, E.; Fleith, G.; Fatisson, J.; Labbé, P.; Voegel, J.-C.; Schaaf, P.; Ball, V. *Langmuir* **2005**, *21*, 3664–9.

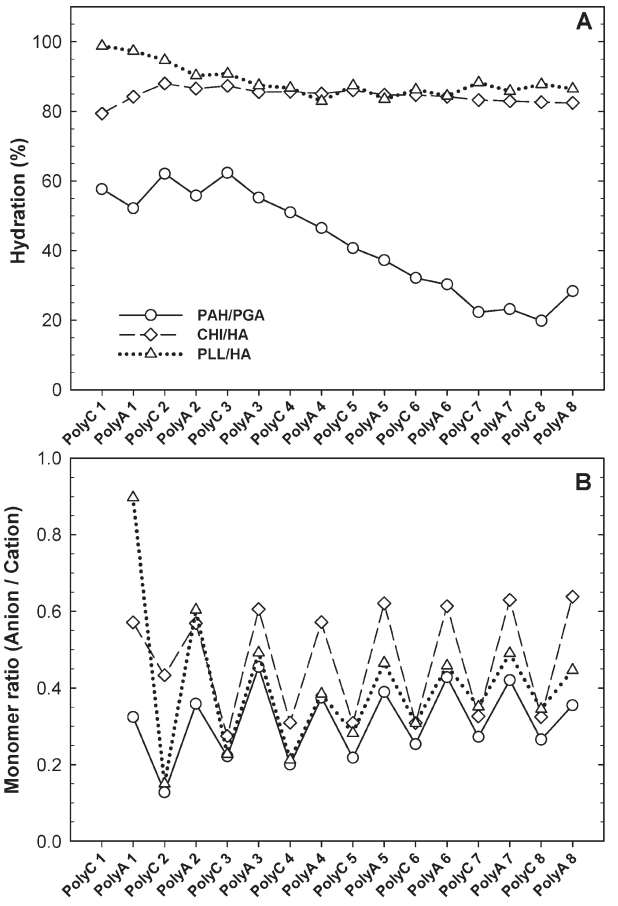

Figure 6. Film hydration (A) and monomer ratio between anion monomer unit and cation monomer unit (B) as a function of the number of deposited layer pairs for the three different types of films: (PAH/PGA) (○), (CHI/HA) (◇), and (PLL/HA) (△). The mean standard deviation of three independent experiments was 0.03 for (PAH/PGA), 0.14 for (CHI/HA), and 0.07 for (PLL/HA) (not shown on the graph for clarity). The continuous, dashed, and dotted lines are plotted to guide the eyes.

was indeed confirmed by confocal laser scanning microscopy observations of the z section of $(PAH/PGA)_8$-PAH^{FITC} films (Figure SI 3). It should also be noted that, in the present case, the nonstoichiometry was not caused by differences in the deposition pH values because all of the polyelectrolytes were fully ionized under our working conditions. It can be effectively observed in Figure 4 that only the COO^- group was visible (not COOH).

Quantitative Film Cross-Linking Monitored by ATR-FTIR Spectroscopy. We further investigated how the internal structure of the different films could be manipulated by introducing covalent cross-links into the films. To this end, we examined how they responded to the presence of a cross-linking agent (EDC) brought into contact with the film after buildup. In previous studies, we showed that this reaction, which involves only carboxylic groups with amine groups, leads to the creation of covalent amide bonds.[27,37] Such bonds can be quantified by ATR-FTIR spectroscopy. We thus monitored the evolution of the ATR-FTIR spectra of films composed of eight-layer pairs after contact with increasing concentrations of EDC. We systematically measured the decrease in the carboxylic peak of PGA or HA, which was directly related to the formation of amide bonds because the reaction had one-to-one stoichiometry between carboxylic and amine groups.[27] The molar densities of the COO^- groups as well as the percent of COO^- groups consumed in the reaction are shown in Figure 7 as a function of the initial EDC concentration for the three film types. The concomitant increase in amide groups is also shown in this Figure.

Table 3. Molar Densities of the Films Based on the Monomeric Units[a]

	polycation μmol/cm^3	polyanion μmol/cm^3	total μmol/cm^3
$(PAH/PGA)_8$	82.3 ± 9.8	26.2 ± 1.9	108.5 ± 3.9
$(CHI/HA)_8$	6.7 ± 0.9	3.1 ± 0.6	9.8 ± 1.3
$(PLL/HA)_8$	6.4 ± 0.8	2.5 ± 0.5	8.9 ± 1.4

[a] These were calculated by dividing the adsorbed amounts determined from ATR-FTIR by the molar mass of the monomer and the film's hydrated thickness as obtained by QCM-D for the three PEM systems studied. The total molar density of the film was obtained by adding the molar densities of each polycation and polyanion.

The curves show a similar trend characterized by an initial increase followed by stabilization toward a plateau value at high EDC concentrations. Note that the $(PAH/PGA)_8$ films had the highest absolute decrease in the molar density of the COO^- groups (Figure 7A), whereas the consumption of these groups expressed as a percentage is lower than for the other films. Thus, whereas 60% of the COO^- groups were engaged in covalent amide bonds for an EDC concentration of 100 mg/mL, this fraction rose to ~80% for $(CHI/HA)_8$ films and ~90% for $(PLL/HA)_8$ films (Figure 7B). In all cases, a fraction of the COO^- groups did not react, presumably because of the steric hindrance and entanglements of the polymer chains. Considering that charge neutrality must be respected in the film, we assume that the remaining "free" COO^- groups were involved in weaker interactions with Na^+ counterions because of the presence of 0.15 M NaCl in the rinsing solutions. Similarly, the total number of ammonium groups was much higher for the $(PAH/PGA)_8$ films than for the other films (Figure 7A′). Only 30 to 50% of the ammonium groups, depending on film type, reacted during the cross-linking reaction (Figure 7B′), which suggests that these groups may interact to a large extent with Cl^- counterions. However, for technical reasons (the counterions present here were not infrared-active), it was not possible to obtain direct proof of their presence, even though the effect of ionic strength on film growth and stability strongly suggested it.[39,49]

The molar density of the amide bonds created is shown in Figure 8. It was much higher for $(PAH/PGA)_8$ films (16.2 μmol/cm^3) than for $(PLL/HA)_8$ (2.2 μmol/cm^3) and $(CHI/HA)_8$ films (2.4 μmol/cm^3) at an EDC concentration of 100 mg/mL. This is an ~7 fold increase for the former as compared to that for the latter. Thus, because of the large initial number of charged COO^- groups incorporated into the films, the (PAH/PGA) films allowed variation of the covalent amide bonds over a wide range.

Mechanical Properties of the Films. Initially, it was predicted that, on the basis of the molar densities and degree of cross-linking obtained by quantitative analysis of the FTIR spectra, the different films would have different mechanical properties. However, apart from covalent cross-linking, the mechanical properties are a combination of several other contributions, including the intrinsic stiffness of the chains, ionic cross-links, and water content. Furthermore, one expects the mechanical properties to depend greatly on the degree of cross-linking, as previously shown for (PLL/HA) films.[37,63] This may also be anticipated for (CHI/HA) films by comparing a native film (i.e., uncross-linked films) with a cross-linked film at an intermediate EDC concentration.

(63) Francius, G.; Hemmerle, J.; Ohayon, J.; Schaaf, P.; Voegel, J.-C.; Picart, C.; Senger, B. *Microsc. Res. Tech.* **2006**, *69*, 84–92.

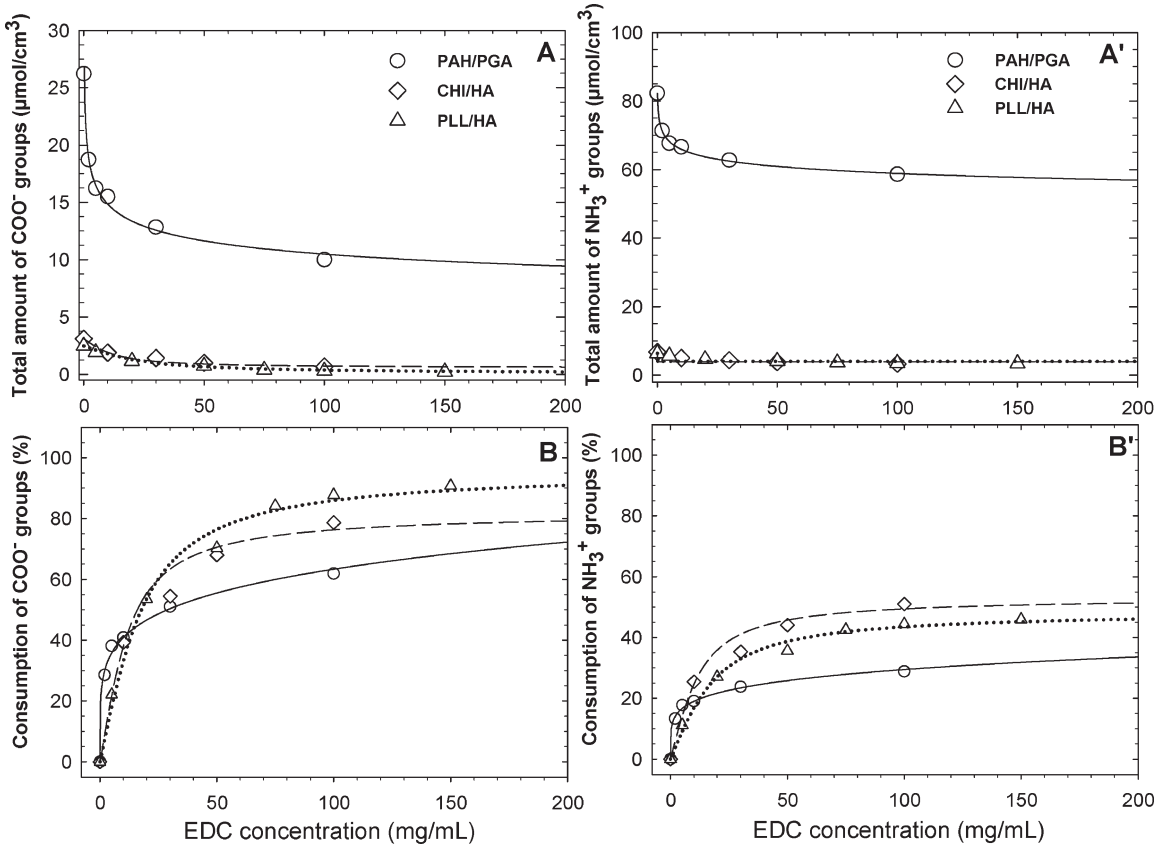

Figure 7. Total numbers of COO^- and NH_3^+ groups as well as their consumption as a function of the initial EDC concentration. The total numbers of COO^- and NH_3^+ groups (A and A′, respectively) are expressed in molar densities (i.e., number of moles per film volume based on the monomeric unit). They were calculated from the ATR-FTIR data using the calibration curves for the determination of the absolute quantities and by quantifying the decrease in the COO^- bands of PGA or HA after cross-linking. For the NH_3^+ groups, the absolute number of groups that have reacted is equal to that of COO^- because of the 1:1 stoichiometry of the cross-linking reaction. The consumption of these groups is expressed as a percentage of the initial molar density (B and B′, respectively) for (PAH/PGA) (○), (CHI/HA) (◇), and (PLL/HA) (△) films. The lines are drawn to guide the eyes.

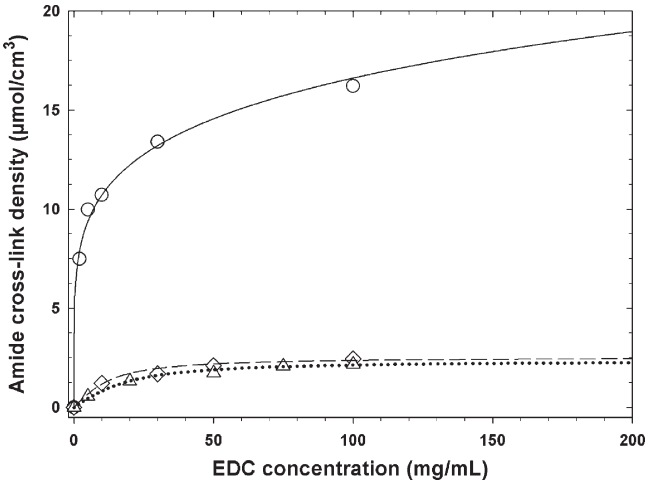

Figure 8. Molar density of covalent amide bonds created upon film cross-linking for (PAH/PGA) (○), (CHI/HA) (◇), and (PLL/HA) (△) films. The lines are drawn to guide the eyes.

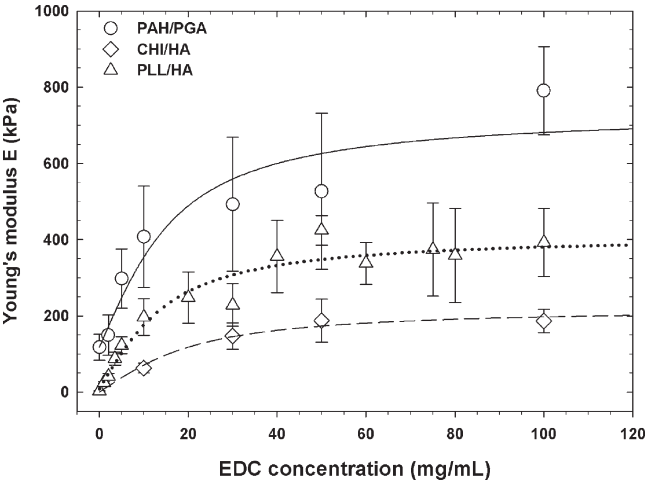

Figure 9. Young's modulus E as a function of the initial EDC concentration for (PAH/PGA) (○), (CHI/HA) (◇), and (PLL/HA) (△) films. E was deduced from nanoindentation curves for the different (PolyC/PolyA) films according to eq 5. The lines are drawn to guide the eyes.

To understand better the influence of the degree of cross-linking on PEM stiffness, we performed nanoindentation experiments using colloidal probe AFM and compared the three film types (Figure 9).

Interestingly, we observed a similar trend (i.e., a stiffening of the film when the EDC concentration increased), followed by stabilization toward a plateau value. This was qualitatively similar to what was observed by FTIR (Figure 8). For (CHI/HA) films, the Young's modulus E increased from 63 ± 12 to 187 ± 31 kPa when the initial EDC concentration was raised from

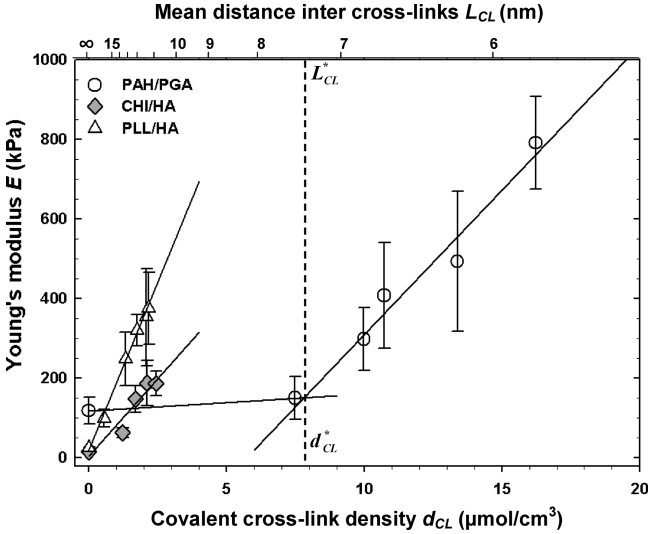

Figure 10. Young's modulus E plotted as a function of cross-link density (lower X axis) and mean distance between cross-links L_{CL} (upper X-axis) for (PAH/PGA) (○), (CHI/HA) (◊), and (PLL/HA) (△) films. The lines correspond to the best linear regression.

10 to 100 mg/mL. The most cross-linked films thus appeared to be ~3 times stiffer than the native films. In agreement with our previous results obtained for a single EDC concentration, we found that the cross-linked (PLL/HA) films were stiffer than the (CHI/HA) films, with E ~2 times higher at an EDC concentration of 100 mg/mL. As anticipated from the FTIR spectroscopy analysis, we found that (PAH/PGA) films were considerably more rigid than (PLL/HA) and (CHI/HA) films for a given EDC concentration. For these films, E spans a wide range from 118 ± 34 kPa for the native films to 791 ± 116 kPa for films cross-linked with an EDC concentration of 100 mg/mL. This is a 2-fold increase as compared to that for (PLL/HA) films and a 4-fold as compared to that for (CHI/HA) films. The greater stiffness for the native (PAH/PGA) films may be due to the presence of α-helices in 30% of the PGA chains[40] because the secondary polyelectrolyte structure is known to influence the films' mechanical properties.[64] The greatest number of ionic cross-links (molar density of the COO^- groups) and the lowest degree of hydration may also play a role. Note that the PLL in (PLL/HA) films is much less structured and has only a random or turn structure.[21]

Correlation between Covalent Cross-Link Density and Mechanical Properties. We subsequently investigated whether there is a correlation between the formation of the amide cross-links and mechanical properties. Such a relationship is indeed already known to exist for macroscopic gels in solution, for which the elasticity (or shear modulus) derived from rheological measurements is found to depend on the cross-linking density.[65] For this purpose, we plotted E as a function of the cross-link's molar density (Figure 10). It should be noted that this graph takes into account only the covalent cross-links that were created upon EDC cross-link molar. Interestingly, two different kinds of behavior emerged. For the (PLL/HA) and (CHI/HA) films, E varied linearly with the cross-link density. Conversely, for (PAH/PGA) films, two-step behavior was observed. For a cross-link density (d_{CL}) lower than $d^*_{CL} \approx 8\ \mu$mol/cm^3, E increased only slightly with the cross-link density (slope of 4.3 kPa/(μmol/cm^3)), but for higher densities, a sharp increase was visible with a slope of 72.6 kPa/(μmol/cm^3). This kind of behavior is somewhat similar to the mechanical behavior of semiflexible polymer networks. Semiflexible polymers are so-called because their characteristic bending length is comparable to other length scales in the problem, such as the contour length or the network mesh size, and thus cannot be neglected.[65] These semiflexible polymer networks are characterized by the existence of qualitatively distinct regimes in the elastic response, separated by a rigidity percolation threshold. Below a critical cross-link density, the elastic deformation of the gel is spatially heterogeneous over long length scales and is dominated by filament bending, leading to a low bulk stiffness. When the cross-link density exceeds the critical value, the strain is guided by the extension/contraction of the polymer chains and becomes uniform throughout the sample.[65] The mechanical behavior of (PAH/PGA) films thus presents a sort of "percolation threshold", except that in the present case the E value of the native films is not zero.

From the molar densities of cross-links, we also estimated the mean distance between covalent cross-links (L_{CL}), which was calculated as the diameter of the sphere of equivalent volume

$$V_{CL} = \frac{1}{d_{CL} N_A} = \frac{4\pi}{3}\left(\frac{L_{CL}}{2}\right)^3 \quad (6)$$

where N_A is the Avogadro constant ($N_A \approx 6.022 \times 10^{23}$). L_{CL} is represented as the top X axis in Figure 10. The critical cross-link density for (PAH/PGA) films above which the Young's modulus sharply increased corresponded to a mean distance L_{CL} of ~7.4 nm. Interestingly, for (PLL/HA) and (CHI/HA) films, the minimal L_{CL} values obtained for the highly cross-linked films were ~11.6 and ~10.9 nm, respectively. For the highly cross-linked (PAH/PGA) films (d_{CL} = 16.2 μmol/cm^3), L_{CL} decreased to ~5.8 nm. The significantly shorter distance between the cross-links in (PAH/PGA) films may have led to more restricted motion in the polyelectrolyte chains. On the contrary, a considerable distance between cross-links, such as in (CHI/HA) and (PLL/HA) films, may be related to higher flexibility.

Conclusions

This work provides the first basis for measuring film hydration and internal composition. For the first time, we have quantified the absolute molar densities of the films as well as the density of covalent cross-links created by means of carbodiimide chemistry. In addition, we measured their mechanical properties over a wide range of cross-link concentrations. There were significant differences between the (PLL/HA), (CHI/HA), and (PAH/PGA) films, which were all characterized by the exponential growth of their thickness. These differences, which were not visible at first glance when taking into consideration only thickness growth, were revealed after an in-depth study of their internal chemical structure and mechanical properties. (CHI/HA) and (PLL/HA) films had similar properties, including a high water content (~81−86%), a low initial density of COO^- groups, and a maximal E modulus that reached 200 and 400 kPa, respectively. Conversely, (PAH/PGA) films emerged as being less hydrated (~ 29%) and much more dense, with ~10 times more COO^- groups in the native films than in the other films. Also, their cross-link density covered a wider range, with up to 16.2 μmol/cm^3 created, which was ~7 times greater than for the (CHI/HA) and (PLL/HA) films. For all three systems studied, film buildup under physiological conditions (i.e., with no internal drying step) showed significant nonstoichiometry with a charge excess on

(64) Schoeler, B.; Delorme, N.; Doench, I.; Sukhorukov, G. B.; Fery, A.; Glinel, K. *Biomacromolecules* **2006**, *7*, 2065–71.
(65) Head, D. A.; Levine, A. J.; MacKintosh, F. C. *Phys. Rev. E: Stat. Phys., Plasmas, Fluids, Relat. Interdiscip. Top.* **2003**, *68*, 061907.

the polycation chains (whether PLL, CHI, or PAH). Gaining insight into the internal composition of PEM films in relation to their mechanical properties contributes to a better understanding of these thin films. These films can be considered to be nanometer, thin two-component hydrogels presenting a much higher concentration of polyelectrolyte chains than their solution (or volumeric) counterparts (polyelectrolyte complexes or macroscopic gels). Future work will be focused on the interplay between the internal composition of the films, their mechanical properties, and cell adhesive properties.

Acknowledgment. This work was supported by the Association Française contre les Myopathies (AFM, grant no. 12671), the Association pour la Recherche sur la Cancer (equipment grant no. 7918), the Fondation Recherche Médicale (equipment grant no. INE20061108297), and the Agence Nationale pour la Recherche (grants ANR-06-NANO-006 and ANR-07-NANO-002). C.P. is a junior member of the Institut Universitaire de France, whose support is gratefully acknowledged. T.C. thanks the AFM for a Ph.D. fellowship.

Supporting Information Available: FTIR calibration spectra and major peak assignments for PLL and HA. Differences in the frequency shifts ($\Delta f/v$) during film growth monitored in situ by QCM-D for the different systems. Vertical section of the $(PAH/PGA)_8$-PAH^{FITC} film obtained from CLSM observations. This material is available free of charge via the Internet at http://pubs.acs.org.